Proceedings of the
International Conference on Mechanical Engineering 2005
(ICME2005) 28- 30 December 2005, Dhaka, Bangladesh

ICME05-FL-04

EFFECT OF HETEROGENEOUS CONDENSATION ON AXISYMMETRIC SUPERSONIC FREE JETS

Toshihiro Nakano[1], MD. Mahbubul Alam[2], Shigeru Matsuo[1], Masanori Tanaka[2] and Toshiaki Setoguchi[1]

[1] Dept. of Mechanical Engineering, Saga University, 1 Honjo-machi, Saga-shi, Saga 840-8502, Japan.
[2] Graduate School of Science and Technology, Saga University, 1 Honjo-machi, Saga-shi, Saga 840-8502.

ABSTRACT

The effect of the heterogeneous condensation on the characteristics of axisymmetric under-expanded jet is investigated numerically. The governing equations are unsteady axisymmetric compressible Navier-Stokes equations with a rate equation of liquid-phase production. As the results, the condensation with the heterogeneous nucleation has a strong effect on the jet structure. Furthermore, it is shown that the condensing flow field with the heterogeneous nucleation is dependent largely on the concentration of solid particles in moist air.

Keywords: Compressible Flow, Supersonic Jet, Heterogeneous Condensation, Simulation.

1. INTRODUCTION

The supersonic free jet has long received much interest from researchers since it has had many potential applications for aeronautical and mechanical industries, and it has also been of importance in academic aspects as well. Much effort has been devoted to the major characteristics of supersonic jets [1, 2, 3, 4, 5, 6]. According to these previous works, the under-expanded supersonic jet is specified by its barrel shock structure, Mach disk location, jet boundary configuration, velocity decay and supersonic length, etc., which are usually determined by the jet pressure ratios [7, 8].

Supersonic moist air jet technologies have been often applied to power plants and industrial manufacturing processes [4, 5]. However, the major features like a Mach disk of the supersonic moist air jet are not well known to date even for its qualitative characteristics.

Condensation phenomenon of moist air or steam in a high speed flow field (transonic or supersonic flow field) is in general induced through the non-equilibrium condensation process. In the process, condensation nuclei are generated by collision and coalescence of vapor molecules, and the condensation of the vapor takes place on the nuclei (homogeneous condensation). On the other hand, in heterogeneous condensation, the condensation of the vapor takes place on foreign nuclei ; smoke and vapor from fires and various industries, dust from land surfaces, salt from oceans and particulate products from chemical reaction [9]. Their presence in sufficient numbers leads to the condensation near to equilibrium at degree of supersaturation slightly larger than unity. The condensation phenomenon like this may occur in the supersonic free jet. However, the detailed flow information is not yet well known for the condensation in the jet flow.

In the present study, the simulations were conducted in order to clarify the effect of the heterogeneous condensation on the characteristics of axisymmetric under-expanded jet.

2. COMPUTATIONAL METHOD

2.1 Governing Equations

Assumptions used in the present calculation are as follows ; Both velocity slip and temperature difference do not exist among condensate droplets, solid particles and inert gas mixture, and the effects of the condensate droplets and solid particles on pressure are neglected. All particles are assumed to have a smooth and spherical shape, and all condensation nuclei are assumed to be chemically inert and insoluble in water vapor.

The governing equations are unsteady, axisymmetric, compressible Navier-Stokes equations and a rate of liquid-phase production with homogeneous and heterogeneous nucleations, and are taken into account simultaneously [10, 11].

They are written in the axisymmetric Cartesian coordinate system (x,y) as follows ;

$$\frac{\partial \boldsymbol{U}}{\partial t}+\frac{\partial \boldsymbol{E}}{\partial x}+\frac{\partial \boldsymbol{F}}{\partial y}=\frac{\partial \boldsymbol{R}}{\partial x}+\frac{\partial \boldsymbol{S}}{\partial y}+\frac{1}{y}\boldsymbol{H}_1+\boldsymbol{H}_2+\boldsymbol{Q} \qquad (1)$$

where $\boldsymbol{U}$ is the vector of conservative variables, $\boldsymbol{E}$ and $\boldsymbol{F}$ are inviscid flux vectors, and $\boldsymbol{R}$ and $\boldsymbol{S}$ are viscous flux vectors. $\boldsymbol{H}_1$, $\boldsymbol{H}_2$, and $\boldsymbol{Q}$ are the source term of axisymmetry, turbulence, and condensation, respectively.

g_{hom} and g_{het} indicate condensate mass fractions generated by homogeneous and heterogeneous nucleations, respectively. Therefore, total flow rate of liquid phase g_{total} [11] is written as

$$g_{total} = g_{hom} + g_{het} \tag{2}$$

Both of the condensate mass fractions g are expressed as a rate equation, based on the following equation [10].

$$\frac{dg}{dt} = \frac{4\pi}{3} \cdot \rho_l \cdot r^*(t)^3 \cdot \frac{I(t)}{\rho_m(t)} + \int_{-\infty}^{t} 4\pi \cdot \rho_l \cdot \frac{I(\tau)}{\rho_m(\tau)} \cdot \frac{\partial r(t,\tau)}{\partial t} \cdot r(t,\tau)^2 \cdot d\tau \tag{3}$$

In Eq.(3), t and τ are the time, respectively. ρ is the density. r, r^*, and I are averaged droplet radius, critical droplet radius, and nucleation rate per unit time and volume. Subscripts m and l refer to mixture and liquid, respectively.

Heterogeneous nucleation process consists of four nucleation stages [11] : I) generation of embryo, II) growth of embryo, III) formation of liquid film, and IV) growth of liquid film. There are two models for heterogeneous nucleation process. For model 1, all stages from I to IV are considered for nucleation process. For model 2, only the fourth stage (IV) of nucleation process is used. This model is assumed that nucleation stages from I to III proceed in an infinitesimal time. In the present study, model 2 was employed because the difference between results obtained by both models is very small [11].

The governing equation systems for compressible viscous flow were discretized by the finite difference method. Third-order TVD finite difference scheme with MUSCL approach [12] was used for spatial derivative terms and second-order central difference scheme in discretizing viscous terms. The spatially discretized equations were integrated in time by means of a time splitting method that had the second order accuracy. A modified k-R model [11, 13, 14, 15] was employed to close the governing equations as a turbulence model.

2.2 Computational Conditions

Figure 1 shows computational grids of flow field. The sonic nozzle with a straight part of 5.08 mm has a diameter of ϕD_n = 12.7 mm (characteristic length). The shape of the nozzle is the same as that used by Addy [16]. The number of grids is 70×60 in the nozzle and 400×120 in the region downstream of nozzle exit.

The pressure ratio which means the ratio of the reservoir pressure p_0 (atmospheric pressure) and back pressure p_b, is denoted by φ (= p_0/p_b). In the present study, values of φ are 3.8 and 6.2. Values of the initial degree of supersaturation S_0 are 0 and 0.7. Total temperature T_0 and total pressure p_0 in the reservoir are 298.15 K and 101.3 kPa, respectively. For the heterogeneous condensation, a radius of particle is 1.0×10^{-8} m [17] and the concentration of the solid particles per unit volume of the moist air in the reservoir $n_{het,0}$ is varied from 1.0×10^{15} m^{-3} to 1.0×10^{17} m^{-3} [11]. The contact angle is fixed at 30 degrees [11].

The non slip-wall, ambient and downstream conditions are use as the boundary conditions (Fig.1). Inlet and exit boundaries are constrained with free boundary condition. Iso-pressure and no heat transfer are constrained on the solid wall. Condensate mass fraction is set at g = 0 on the wall.

In the present study, the fineness and number of computational grids were examined to assure that the obtained solutions were independent of the grid employed, and the grid provided reasonable predictions.

3. RESULTS AND DISCUSSION

Figures 2 and 3 show the typical contour maps of density in case of φ = 3.8 and 6.2, respectively. For the pressure ratios applied, the jet is under-expanded at the exit of nozzle. Figures 2(a) and 3(a) show density contour maps for dry air (S_0 = 0), and Figs. 2(b) and 3(b) show for moist air with homogeneous condensation (S_0 = 0.7), respectively. Contour maps of density for heterogeneous condensation are shown in Fig.2(c) ($n_{het,0}$ = 1.0×10^{17} m^{-3}, S_0 = 0.7) and Fig.3(c) ($n_{het,0}$ = 1.0×10^{17} m^{-3}, S_0 = 0.7).

In Fig.2(b), density gradient in an expansion fan is slightly changed in comparison with the case of dry air (Fig.2(a)) due to the latent heat released by the homogeneous condensation. Furthermore, Mach disk appears at the position x/D_n = 1.16. In Fig.3(b), there is little change for the position of Mach disk from the nozzle exit. However, the diameter of Mach disk becomes large in comparison with that in Fig.3(a).

For heterogeneous condensation in Figs.2(c) and 3(c), density gradients are not seen in an expansion fan, and the diameter of Mach disk becomes small compared with the case of the homogeneous condensation (Figs.2(b) and 3(b)). However, there is not much change for the position of Mach disk from the nozzle exit.

Figures 4(a) and 4(b) show the contour maps of condensate mass fraction in the flow field corresponding to Figs.2(b) and 2(c), respectively. In Fig.4(a), the

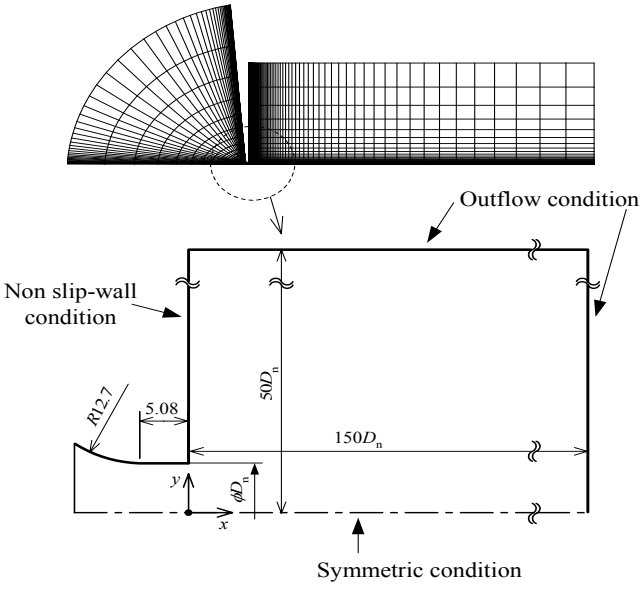

Fig 1. Computational grids (Unit : mm)

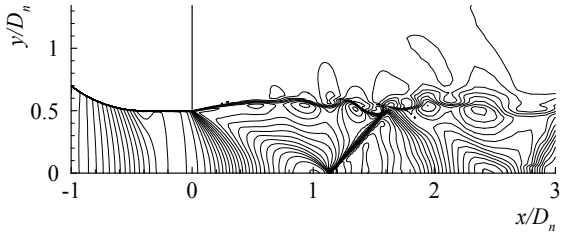

(a) Without condensation ($S_0 = 0$)

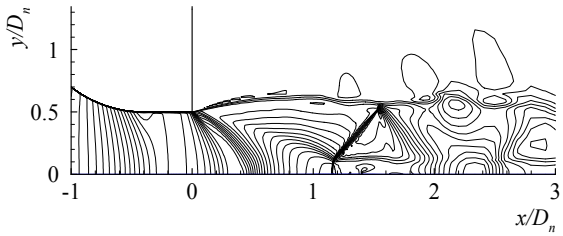

(b) Homogeneous condensation ($S_0 = 0.7$)

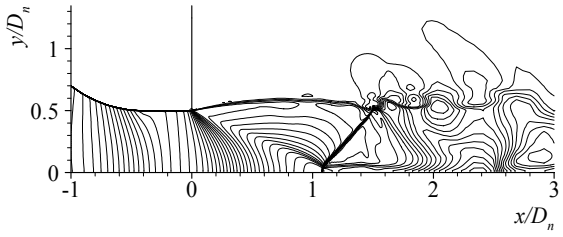

(c) Heterogeneous condensation
($S_0 = 0.7$, $n_{het,0} = 1.0\times10^{17}$ m^{-3})

Fig 2. Contour maps of density ($\varphi = 3.8$)

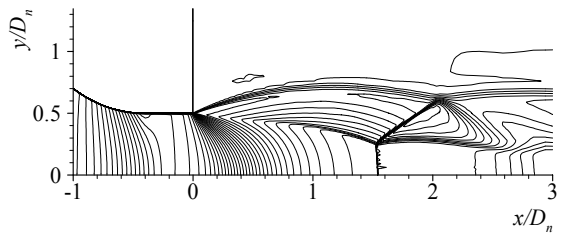

(a) Without condensation ($S_0 = 0$)

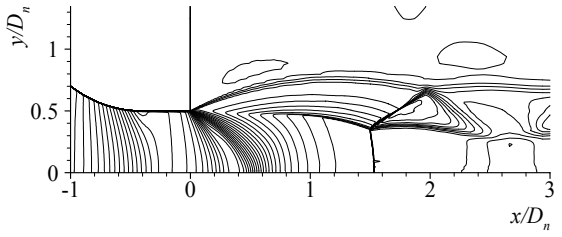

(b) Homogeneous condensation ($S_0 = 0.7$)

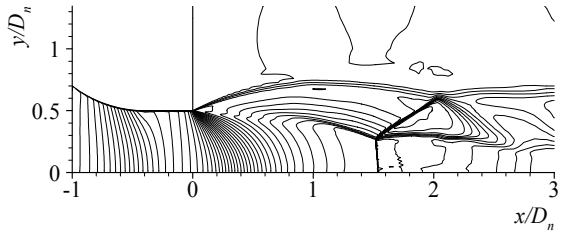

(c) Heterogeneous condensation
($S_0 = 0.7$, $n_{het,0} = 1.0\times10^{17}$ m^{-3})

Fig 3. Contour maps of density ($\varphi = 6.2$)

condensate mass fraction increases rapidly in an expansion fan. However, in Fig.4(b), it increases from upstream of the nozzle exit and there is little increase of condensate mass fraction in an expansion fan. In case of the pressure ratio $\varphi = 6.2$ shown in Fig.5, the tendency of the distributions of condensate mass fraction is almost same to the case of $\varphi = 3.8$.

Figure 6 shows the distributions of static pressure, condensate mass fraction and nucleation rate on the nozzle center line in the case of $\varphi = 3.8$. A static pressure distribution for S_0=0 (dotted line) is also shown in each figure, for reference. In Fig.6(a) (homogeneous condensation), the nucleation rate reaches maximum downstream of the nozzle exit and the condensate mass fraction increases from the maximum position. In Fig.6(b), it is found that onset of condensation moves upstream, and the occurrence of nuclei by the homogeneous condensation is not seen upstream of nozzle exit. Furthermore, condensate mass fraction generated by heterogeneous condensation becomes dominant.

Figure 7 shows the distributions of static pressure, condensate mass fraction and nucleation rate on the nozzle center line in the case of $\varphi = 6.2$. The tendency of the distributions of condensation properties are almost same to the case of $\varphi = 3.8$. The strength of the Mach disk in Figs.7(a) and (b) seems to become weak slightly in comparison with case of dry air ($S_0 = 0$). The static pressure in Fig.7(b) becomes large upstream of the nozzle exit in comparison with the case of Fig.7(a). This is due to the latent heat released by the heterogeneous condensation.

Figure 8 shows the Mach disk diameter (D_{md}) and the distance (L_{md}) from nozzle exit corresponding to each pressure ratio. Results obtained from experiments of Addy [16] are also shown, for reference. Computational results for $\varphi = 3.8$ and 6.2 are shown in cases of $n_{het,0}$=1.0×10^{15} m^{-3}, 1.0×10^{16} m^{-3} and 1.0×10^{17} m^{-3}. As seen from this figure, in the case of $\varphi = 3.8$, an increase of the concentration of the solid particles $n_{het,0}$ decreases the Mach disk diameter in comparison with the case of homogeneous condensation and make the Mach disk

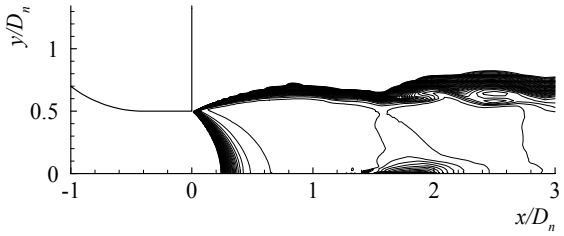

(a) Homogeneous condensation (S_0 = 0.7)

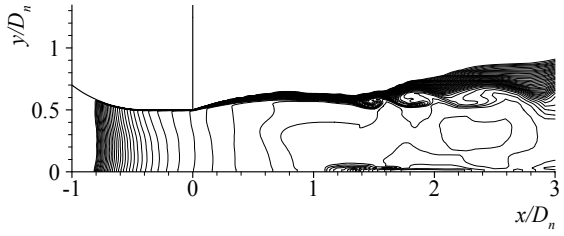

(b) Heterogeneous condensation
(S_0 = 0.7, $n_{het,0}$ = 1.0×10^{17} m^{-3})

Fig 4. Contour maps of condensate mass fraction
(φ = 3.8, S_0 = 0.7)

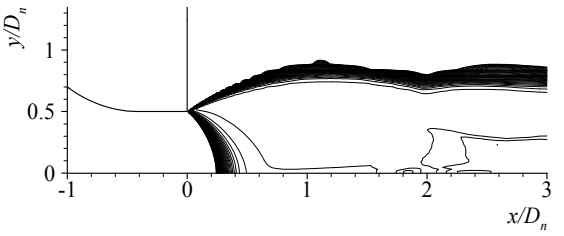

(a) Homogeneous condensation (S_0 = 0.7)

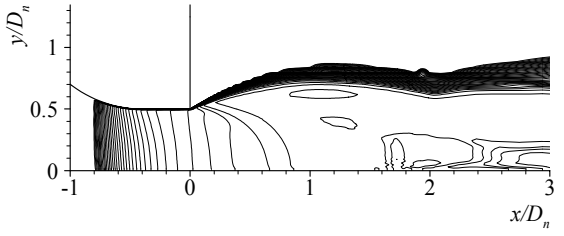

(b) Heterogeneous condensation
(S_0 = 0.7, $n_{het,0}$ = 1.0×10^{17} m^{-3})

Fig 5. Contour maps of condensate mass fraction
(φ = 6.2, S_0 = 0.7)

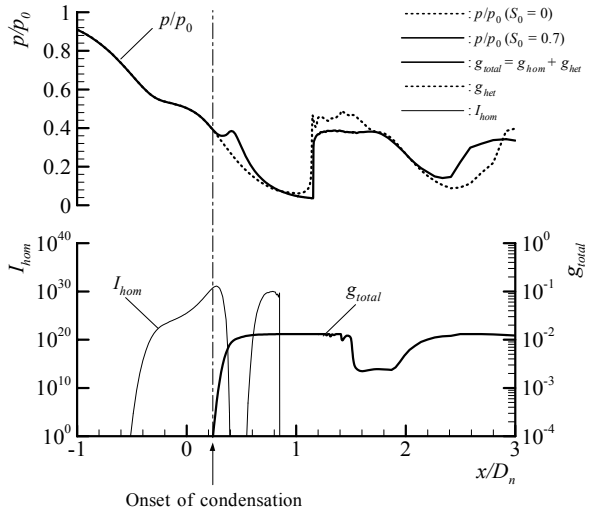

(a) Homogeneous condensation

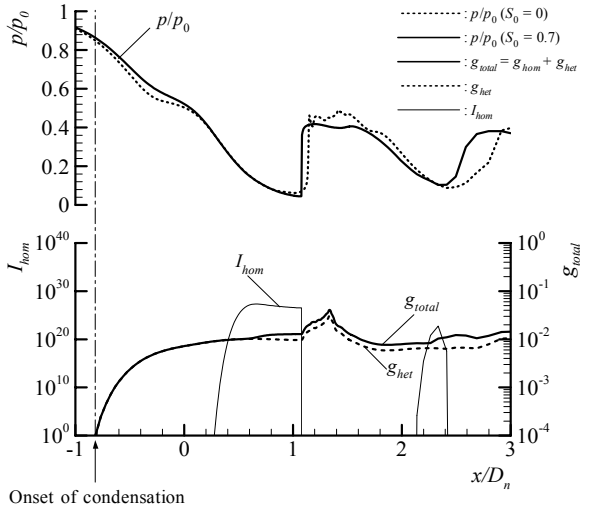

(b) Heterogeneous condensation ($n_{het,0}$ = 1.0×10^{17} m^{-3})

Fig. 6. Distributions of static pressure, condensate mass fraction and nucleation rate (φ = 3.8, S_0 = 0.7)

location move upstream. On the other hand, in the case of φ = 6.2, the Mach disk diameter decreases with $n_{het,0}$, and the diameter for $n_{het,0}$= 1.0×10^{17} m^{-3} is almost the same as that for S_0 = 0 (dry air). But increase of the concentration of the solid particles $n_{het,0}$ does not have an influence upon the Mach disk location.

Figure 9 shows the distributions of total pressure loss at the position of x/D_n=1.5 for φ = 3.8(see Fig.2). Total pressure losses for the case of homogeneous condensation become large due to generation of Mach disk (y/D_n < 0.16) in comparison with case of dry air (S_0 = 0). For the case of $n_{het,0}$ = 1.0×10^{17} m^{-3}, the total pressure losses due to the Mach disk (0.05 < y/D_n < 0.16) becomes small in comparison with the case of homogeneous condensation because Mach disk becomes small. The total pressure losses due to the heterogeneous condensation (y/D_n > 0.3) are almost the same as the case of homogeneous condensation.

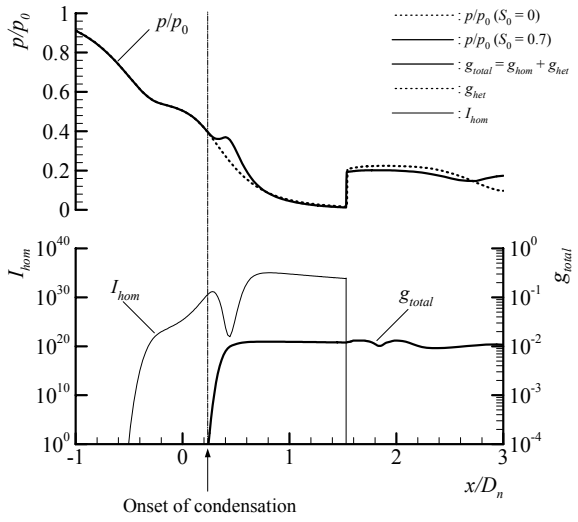

(a) Homogeneous condensation

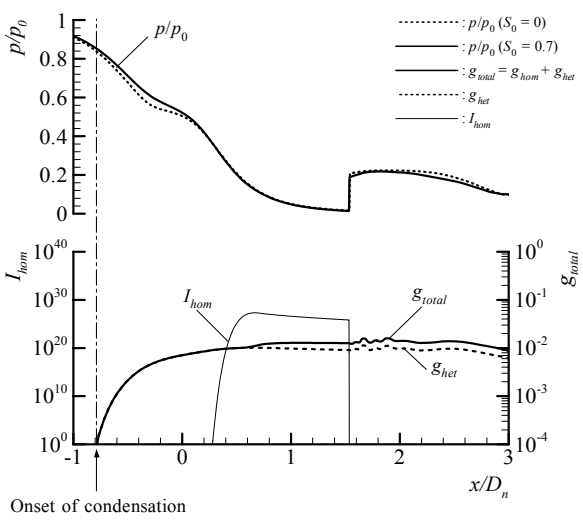

(b) Heterogeneous condensation ($n_{het,0} = 1.0\times10^{17}$ m^{-3})

Fig. 7. Distributions of static pressure, condensate mass fraction and nucleation rate ($\varphi = 6.2$, $S_0 = 0.7$)

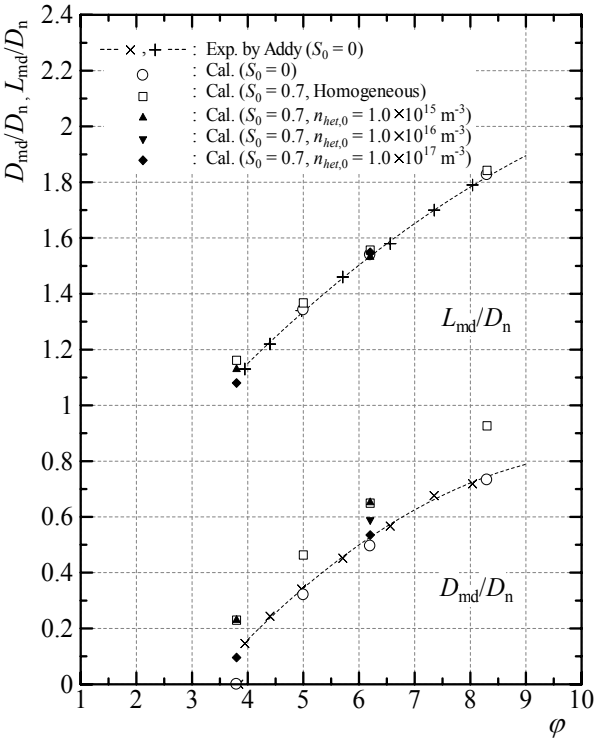

Fig. 8. Diameters and locations of Mach disk

Figure 10 shows the distributions of total pressure loss at the position of x/D_n=2.0 for $\varphi = 6.2$(see Fig.3). Total pressure losses for condensing flows are small behind the Mach disk ($y/D_n < 0.25$) in comparison with case of dry air ($S_0 = 0$). This is considered to be due to reduction in the strength of Mach disk. The total pressure loss on the center line is the smallest for $n_{het,0} = 1.0\times10^{17}$ m^{-3}, and it decreases about 10.1 % compared with the case of dry air.

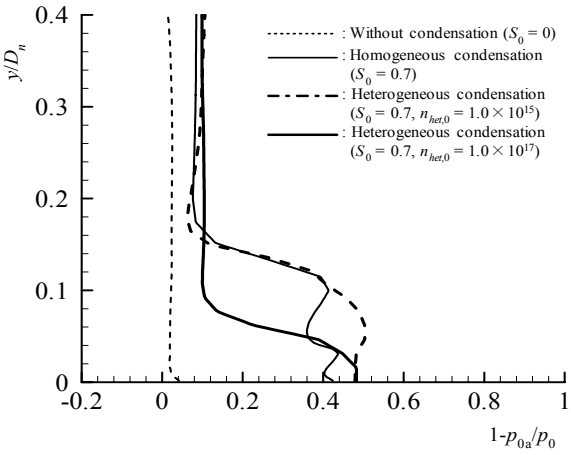

Fig. 9. Distributions of total pressure loss ($\varphi = 3.8$, $x/D_n = 1.5$)

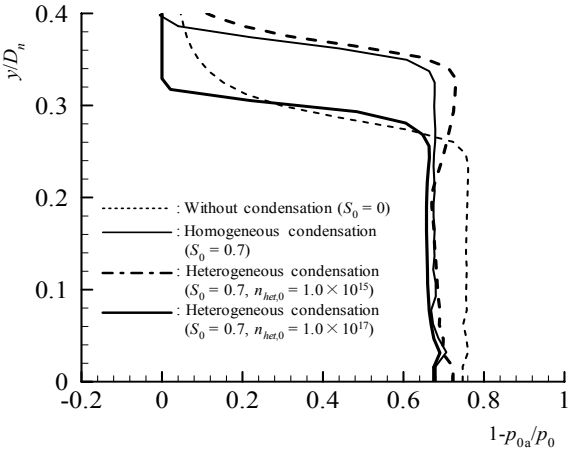

Fig 10. Distributions of total pressure loss ($\varphi = 6.2$, $x/D_n = 2.0$)

4. CONCLUSIONS

Numerical computations have been performed to investigate the effect of the heterogeneous condensation on the characteristics of axisymmetric under-expanded jet. As a result, in the case of low pressure ratio, the diameter of Mach disk decreases with the concentration of the solid particles, and the position of Mach disk moves upstream in comparison with that in dry air jets. Furthermore, total pressure losses for condensing flows become large in comparison with the case of dry air, but it is small in comparison with the case of homogeneous condensation. In the case of high pressure ratio, although the diameter of Mach disk decreases with the concentration of the solid particles, the position of Mach disk is almost the same as that in dry air jet, and total pressure losses for condensing flows become small behind the Mach disk in comparison with case of dry air due to reduction in the strength of the Mach disk.

5. REFERENCES

1. Love, E.S., Grigsby, D.E., Lee, L.P., and Woodling, L.S., 1959, "Experimental and Theoretical Studies of Axisymmetric Free Jets", NASA TR R-6.
2. Sheeran, W., and Dosanjh, D., 1968, "Observations on Jet Flows from a Two-Dimensional, Underexpanded, Sonic Nozzle", AIAA Journal, 6:540-542.
3. Chang, I.S., and Chow, W.L., 1974, "Mach Disk from Underexpanded Axisymmetric Nozzle Flow", AIAA Journal, 12:1079-1082.
4. Kim, H.D., and Shin, H.S., 1996, "Numerical Study on Under-Expanded Jets through a Supersonic Nozzle(part 2)", Journal of Korea Society of Mechanical Engineers Series (B), 20:1994-2004.
5. Kim, H.D. and Lee, J.S., 1996, "An Experimental Study on Supersonic Jet Issuing from Gas Atomizing Nozzle (part 1)", Journal of Korea Society of Mechanical Engineers Series (B), 20:677-709.
6. Mate, B., Graur, I.A., Elizarova, T., Chirokov, I., Tejeda, G., Fernandez, J.M., and Montero, S., 2001, "Experimental and Numerical Investigation of an Axisymmetric Supersonic Jet", Journal of Fluid Mechanics, 426:177-197.
7. Abbett, M., 1971, "Mach Disk in Underexpanded Exhaust Plumes", AIAA Journal, 9:512-514.
8. Davidor, W., and Penner, S.S., 1971, "Shock Standoff Distance and Mach Disk Diameters in Underexpanded Sonic Jets", AIAA Journal, 9: 1651-1652.
9. Kotake. S and Gass, I.I., 1981, "Flows with Nucleation and Condensation", Prog. Aerospace Science, 19:129-196.
10. Sislian, J.P., 1975, "Condensation of Water Vapor with or without a Carrier Gas in a Shock Tube", UTIAS Report, No. 201.
11. Heiler, M., 1999, "Instationäre Phänomene in homogen/heterogen kondensierenden Düsen- und Turbinenströmungen", Dissertation, Fakultät für Maschinenbau, Universität Karlsruhe (TH), Germany.
12. Yee, H.C., 1989, "A class of high-resolution explicit and implicit shock capturing methods", NASA TM-89464.
13. Goldberg, U.C., 1994, "Toward a Pointwise Turbulence Model for Wall-Bounded and Free Shear Flows", Journal of Fluids Engineering, 116: 72-76.
14. Goldberg, U.C., 1996, "Exploring a Three-Equation *R*-*k*-ε Turbulence Model", Journal of Fluids Engineering, 118:795-799.
15. Yamamoto, S. and Daiguji, H., 1991, "Unsteady Navier-Stokes Simulation of Turbulent Flows through a Supersonic Compressor Cascade", ASME FED, 120:73-79.
16. Addy, A.L., 1981, "Effects of Axisymmetric Sonic Nozzle Geometry on Mach Disk Characteristics", AIAA Journal, 19:121-122.
17. Kotake, S. and Glass, I. I., 1976, "Condensation of water vapour on heterogeneous nuclei in a shock tube", UTIAS Report, No.207.

6. NOMENCLATURE

Symbol	Meaning	Unit
D_n	Diameter of nozzle exit	(mm)
D_{md}	Diameter of Mach disk	(mm)
$\boldsymbol{E}$, $\boldsymbol{F}$	Inviscid flux vectors	(-)
g	Condensate mass fraction	(-)
$\boldsymbol{H}_1$	Source term of axisymmetric	(-)
$\boldsymbol{H}_2$	Source term of *k*-*R* model	(-)
I	Nucleation rate per unit time and volume	$(1/s \cdot m^3)$
L_{md}	Distance from nozzle exit to Mach disk position	(mm)
$n_{het,0}$	The concentration of the solid particles per unit volume of the moist air in the reservoir	(m^{-3})
p	Pressure	(Pa)
$\boldsymbol{Q}$	Source term of condensation	(-)
r	Radius	(m)
r^*	Critical radius	(m)
$\boldsymbol{R}$, $\boldsymbol{S}$	Viscous flux vectors	(-)
S	Degree of supersaturation	(-)
t	Time	(s)
T	Temperature	(K)
$\boldsymbol{U}$	Conservative vector	(-)
x, y	Cartesian coordinates	(m)
Symbols		
φ	Pressure ratio	(-)
ρ	Density	(kg/m^3)
τ	Time	(s)
Subscripts		
0	Stagnation	
0a	Local	
b	Back chamber	
hom	Homogeneous	
het	Heterogeneous	
l	Liquid	
m	Mixture	
total	Total	